

# A localization transition underlies the mode-coupling crossover of glasses

D. Coslovich<sup>1\*</sup>, A. Ninarello<sup>1,2</sup>, L. Berthier<sup>1</sup>

**1** Laboratoire Charles Coulomb (L2C), Université de Montpellier, CNRS, Montpellier, France

**2** CNR-ISC, UOS Sapienza, Piazzale A. Moro 2, 00185 Roma, Italy

\* danièle.coslovich@umontpellier.fr

July 19, 2022

## Abstract

We study the equilibrium statistical properties of the potential energy landscape of several glass models in a temperature regime so far inaccessible to computer simulations. We show that unstable modes of the stationary points undergo a localization transition in real space close to the mode-coupling crossover temperature determined from the dynamics. The concentration of localized unstable modes found at low temperature is a non-universal, finite dimensional feature not captured by mean-field glass theory. Our analysis reconciles previous conflicting numerical results and provides a characteristic temperature for glassy dynamics that unambiguously locates the mode-coupling crossover.

## 1 Introduction

The formation of a glass from the supercooled melt results from a giant increase of the structural relaxation time when the temperature drops below the melting point [1, 2]. Whether the slowing down of molecular motion is driven by a single or several physical mechanisms, active over distinct temperature regimes, is still unclear. Available theories are all but unanimous [3, 4], while experiments and simulations, despite recent technical and numerical advances [5], struggle to disentangle theoretical predictions on the sole basis of relaxation data. The existence of a temperature crossover separating two physical regimes of dynamic relaxation is supported by a number of empirical observations and models, but is subject to lively debates [4]. This crossover is described as an avoided dynamic singularity by mode-coupling [6] and mean-field [7] theories of glasses.

In the early 2000's, a series of studies [8–13] suggested that this smooth dynamic crossover originates from an underlying sharp geometric transition characterizing the potential energy surface (PES). Physically, the transition is between a high-temperature regime where the dynamics takes place near unstable saddle modes and a low-temperature one where dynamics is activated between energy minima. In mean-field glass models, a geometric transition is analytically found: below a critical energy level, the closest stationary point to a typical configuration on the PES is not a saddle anymore but a local minimum [14, 15]. The existence of a geometric transition was reported for several liquids with soft interactions, with universal characteristics [9–12, 16]. However, these results have been criticized at the methodological [17,

Table 1: Mode-coupling temperatures  $T_{MCT}$ , localization transition temperatures  $T_\lambda$  and threshold energies  $e_{th}$ . Note that for the network liquid no localization transition could be found.

	$T_{MCT}$	$T_\lambda$	$A_\lambda$	$e_{th}$
50-50 soft spheres	0.20 [28]	$0.197 \pm 0.001$	$11.6 \pm 0.3$	1.74
Ternary mixture	0.288 [27]	$0.278 \pm 0.002$	$17.8 \pm 0.4$	1.08
Network liquid	0.31 [28]	—	—	—
Polydisperse particles $n = 18$	0.50 [27]	$0.460 \pm 0.002$	$20.1 \pm 0.4$	1.47
Polydisperse particles $n = 12$	0.104 [27]	$0.086 \pm 0.002$	$3.4 \pm 0.3$	0.22

[18] and conceptual levels [19], and subsequent studies did not find a transition [20–23], but the transition temperature could not be easily crossed. From these conflicting results it is difficult to draw firm conclusions on the nature the mode-coupling crossover in actual three-dimensional liquids.

Here, we resolve these contradictions and clarify the nature of the change of the PES associated to the mode-coupling crossover in finite dimensions. Our work builds on two key enabling factors, respectively algorithmic and conceptual. The first key feature of our work is the use an efficient swap Monte Carlo algorithm [24, 25], which enables us to probe the landscape properties on both sides of the mode-coupling crossover temperature [26, 27]. Second, we recognize that the geometric transition, as obtained in mean-field models, can only concern the subset of unstable directions on the PES that correspond to *delocalized* displacements, which involve a finite fraction of particles. Previous studies of the statistics of stationary points have considered instead all unstable modes, irrespective of their spatial characteristics. Our analysis demonstrates that a geometric transition occurs only for delocalized modes and that the mode-coupling temperature crossover therefore coincides with a localization transition of the unstable directions of the PES. We argue that the extent to which the mode-coupling singularity is avoided in real liquids is controlled by the concentration of *localized* modes (involving a finite number of particles), which is found to be system-dependent.

## 2 Methods

We determined stationary and quasi-stationary points of the potential energy surface (PES) for systems of  $N$  point particles by minimizing the total squared force

$$W = \frac{1}{N} \sum_{i=1}^N |\vec{f}_i|^2 \quad (1)$$

where  $\vec{f}_i$  is the force on particle  $i$ . Minimizations start from instantaneous configurations obtained from Monte Carlo or molecular dynamics simulations at a given number density  $\rho = N/V$  and temperature  $T$ . For each configuration, we used the l-BFGS minimization algorithm [29] to minimize  $W$ . It is well-known that  $W$ -minimizations locate *true* stationary points only rarely [30] and that the vast majority of points determined with this method are quasi-stationary points, at which there is precisely one inflection mode having a null zero eigenvalue [18]. In our minimizations, this inflection mode has a nearly zero eigenvalue whose

norm  $|\lambda|$  is typically between  $10^{-6}$  and  $10^{-4}$  (in the corresponding reduced units, see below) and which is clearly distinguishable from the lowest non-zero eigenvalue for the system sizes used in this work. The inflection mode was removed from the analysis, to avoid spurious  $O(1/N)$  finite size effects when the fraction of unstable modes gets close to zero.

The stationary and quasi-stationary points can be distinguished from the corresponding value of  $W$  (in reduced units), which is low but non-zero for quasi-stationary points and zero within machine precision for true stationary points ( $W \sim 10^{-14}$ ). In practice, we use a threshold of  $\sim 10^{-10}$  to classify the two kinds of points for all models except for the polydisperse spheres with  $n = 12$  (see below), for which a slightly higher threshold is used ( $3 \times 10^{-9}$ ) to account for a less strict convergence criterion on  $W$ -minimizations. Previous studies showed that the statistical properties of quasi-stationary points and stationary points are practically indistinguishable above  $T_{MCT}$  [30]. We further discuss the similarity of these two kinds of points in the Appendix.

### 3 Models

#### 3.1 50-50 soft spheres

This is the historical 50:50 binary mixture introduced by Bernu *et al.* [31]. The pair interaction potential is

$$u_{\alpha\beta}(r) = \epsilon \left( \frac{\sigma_{\alpha\beta}}{r} \right)^{12} \quad (2)$$

where  $\alpha, \beta = A, B$  are species indexes. The size ratio is  $\frac{\sigma_{AA}}{\sigma_{BB}} = 1.2$  and the cross-interaction term is additive  $\sigma_{AB} = (\sigma_{AA} + \sigma_{BB})/2$ . The potential is cutoff and shifted at a distance  $r_{cut} = \sqrt{3}\sigma_{AA}$  by adding a cubic term that ensures continuity of the potential up to the second derivative at  $r_{cut}$  [11, 25]. Energies and distances are expressed in units of  $\epsilon$  and  $\sigma_{AA}$ , respectively. We used configurations from previous molecular dynamics simulations for  $N$  particles at a number density  $\rho = N/V = 1$ , with  $N = 400, 800, 2000$  [28].

#### 3.2 Ternary mixture

The ternary mixture model studied in this work was introduced by Gutierrez *et al.* in Ref. [32]. The interaction potential is given by inverse power laws with an exponent 12, plus additional terms that ensure continuity of the derivatives at the cutoff:

$$u_{\alpha\beta}(r) = \left( \frac{\sigma_{\alpha\beta}}{r} \right)^{12} + c_4 \left( \frac{\sigma_{\alpha\beta}}{r} \right)^{-4} + c_2 \left( \frac{\sigma_{\alpha\beta}}{r} \right)^{-2} + c_0 \quad (3)$$

where  $\alpha, \beta = A, B, C$ . The expressions for  $c_0$ ,  $c_2$ , and  $c_4$  are given in [33]. The size ratio between two species is  $\frac{\sigma_{AA}}{\sigma_{BB}} = \frac{\sigma_{BB}}{\sigma_{CC}} = 1.25$ , with additive cross-interactions, and the chemical compositions are  $x_A = 0.55$ ,  $x_B = 0.30$ , and  $x_C = 0.15$ . The potential is cut off at a distance  $r_{cut} = 1.25\sigma_{\alpha\beta}$ . We performed swap Monte Carlo simulations for  $N = 250, 500, 1500, 3000$  particles at a number density  $\rho = 1.1$ . We used 80% of displacement moves over cubes of side  $0.14\sigma_{AA}$  and 20% of swap moves [27]. To save computational time, we never attempted to exchange the identity of species  $A$  and  $C$ . We note that this model liquid can be equilibrated with swap Monte Carlo below the mode-coupling temperature  $T_{MCT} = 0.29$  [27]. However, because of its crystallization tendency at low temperature, we could not simulate the

metastable liquid with  $N = 1500$  particles for  $T < 0.27$  and the one with  $N = 3000$  particles for  $T < 0.28$ . Energies and distances are expressed in units of  $\epsilon$  and  $\sigma_{AA}$ , respectively.

### 3.3 Network liquid

The network liquid model is a simple binary mixture that mimics the structure and dynamics of silica [34]. The interaction potential between unlike species ( $\alpha \neq \beta$ ) is of the Lennard-Jones type

$$u_{\alpha\beta}(r) = 4\epsilon_{\alpha\beta} \left[ \left( \frac{\sigma_{\alpha\beta}}{r} \right)^{12} - \left( \frac{\sigma_{\alpha\beta}}{r} \right)^6 \right] \quad (4)$$

while the one between equal species is a simple inverse power

$$u_{\alpha\alpha} = \epsilon_{12}(\sigma/r)^{12} \quad (5)$$

Energies and distances are expressed in units of  $\epsilon_{AA}$  and  $\sigma_{AA}$ , respectively. The remaining interaction parameters are  $\epsilon_{AB} = 6$ ,  $\sigma_{AB} = 0.49$ ,  $\sigma_{BB} = 0.85$ ,  $\epsilon_{BB} = 1$ . The potential is cut off smoothly at  $r_{cut}$  by adding a cubic term that ensures continuity of the second derivative at the cut off distance  $r_{cut}$ , as for the soft sphere mixture [11]. The resulting cut-off distances are 2.07692, 1.39081, 1.76538 for  $A - A$ ,  $A - B$  and  $B - B$  interactions, respectively. We analyzed simulations for system sizes  $N = 400, 800, 2000$  at a number density  $\rho = 1.655$  obtained from previous molecular dynamics simulations [28].

### 3.4 Polydisperse particles n=18

We consider the model of polydisperse repulsive particles with additive interactions studied in Ref. [27]. The interaction potential between particles  $i$  and  $j$  is

$$u(r_{ij}) = \epsilon(\sigma_{ij}/r_{ij})^n + c_4 \left( \frac{r_{ij}}{\sigma_{ij}} \right)^4 + c_2 \left( \frac{r_{ij}}{\sigma_{ij}} \right)^2 + c_0 \quad (6)$$

with  $n = 18$  and  $\sigma_{ij} = (\sigma_i + \sigma_j)/2$ . The coefficients  $c_0$ ,  $c_2$ ,  $c_4$  are determined to ensure continuity of the potential at the cut-off distance  $r_{cut} = 1.25\sigma_{ij}$ , as for the ternary mixture. The distribution of particle diameters is  $P(\sigma) = A/\sigma^3$  for  $\sigma_{max} \leq \sigma \leq \sigma_{min}$  and 0 otherwise, with  $A$  a normalization constant. We use  $\sigma_{max}/\sigma_{min} = 2.219$ , which implies a root mean square deviation of the diameter

$$\delta = \frac{\sqrt{\langle \sigma^2 \rangle - \langle \sigma \rangle^2}}{\langle \sigma \rangle}, \quad (7)$$

of about 23%. We simulated systems composed of  $N = 500, 1000, 1500$  particles at a number density  $\rho = 1$  using the swap Monte Carlo algorithm described in Ref. [27].

### 3.5 Polydisperse particles n=12

This is a variant of the polydisperse mixture introduced in the previous section. It features non-additive interactions to stabilize the fluid against phase separation [27]. The interaction potential between particles  $i$  and  $j$  is

$$u(r_{ij}) = \epsilon(\sigma_{ij}/r_{ij})^n + c_4 \left( \frac{r_{ij}}{\sigma_{ij}} \right)^4 + c_2 \left( \frac{r_{ij}}{\sigma_{ij}} \right)^2 + c_0 \quad (8)$$

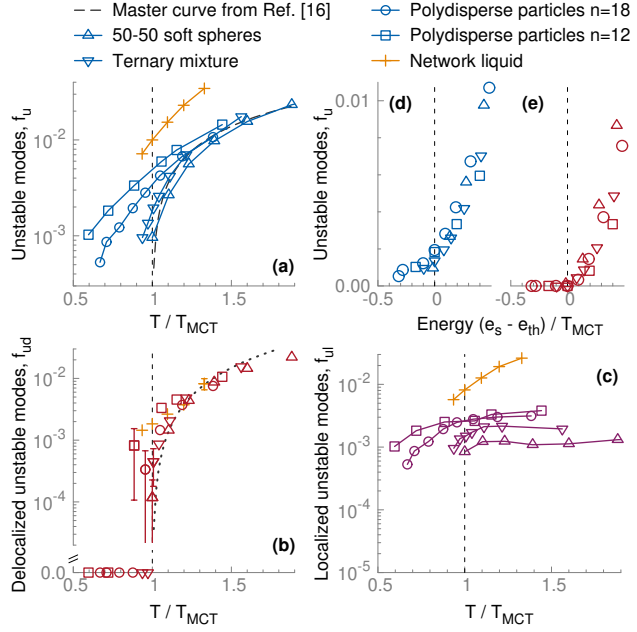


Figure 1: Fractions of unstable modes in stationary and quasi-stationary points for all studied models. Rescaled temperature dependence of (a) total fraction  $f_u$  of unstable modes with dashed line from Ref. [16]. (b) Fraction  $f_{ud}$  of delocalized unstable modes. The dotted line is Eq. (9) with  $f_0 = 0.042$ . Error bars are shown when the relative error exceeds 20%. (c) Fraction of localized modes. (d)  $f_u$  as a function of the scaled energy  $(e_s - e_{th})/T_{MCT}$  of the stationary points. Temperature is used as an implicit variable. (e) Same as (d) for delocalized modes.

with  $n = 12$  and  $\sigma_{ij} = (1 - 0.2|\sigma_i - \sigma_j|)(\sigma_i + \sigma_j)/2$ . The coefficients  $c_0, c_2, c_4$  are determined to ensure continuity of the potential at the cut-off distance  $r_{cut} = 1.25\sigma_{ij}$ . We use  $\sigma_{max}/\sigma_{min} = 2.219$  which implies  $\delta \approx 23\%$ . We simulated systems composed of  $N = 500, 1000, 1500$  particles at a number density  $\rho = 1$  using the swap Monte Carlo algorithm described in Ref. [27].

## 4 Results

We first present our central result and then provide its numerical support. Further details are given in the accompanying data set [35]. In Fig. 1 we show results of force-minimizations that locate stationary and quasi-stationary points of the PES (the distinction between these two families [18] does not affect our conclusions, see Appendix). Diagonalization of the Hessian matrix yields a set of  $3N$  eigenmodes, of which  $n_u$  corresponds to negative eigenvalues  $\lambda$ , i.e., to unstable directions. The top panel shows the corresponding average fraction of unstable modes  $f_u = n_u/(3N)$  as a function of temperature  $T$  for all the models of glass-forming liquids we investigated. Most of these models have been equilibrated below their respective MCT crossover temperatures  $T_{MCT}$ , as determined from power-law fits of the relaxation time data [27, 34]. We are thus in a position to probe the landscape properties in a temperature range inaccessible to previous studies. At low temperature, we observe marked

system-dependent deviations from an empirical power-law singularity introduced in Ref. [16]. Most importantly, the fraction of unstable modes is insensitive to the crossover and remains finite far below  $T_{\text{MCT}}$ , with barely any system-size dependence (see [35]).

The picture changes qualitatively when the spatial localization of the modes is taken into account. As described below, we distinguish between localized and delocalized unstable modes via a finite size scaling analysis of the participation ratio. The fraction of delocalized unstable modes,  $f_{ud}$ , goes strictly to zero when the temperature drops below  $T_{\text{MCT}}$ , see Fig. 1(b). The approach to  $T_{\text{MCT}}$  can be described approximately by the following power law

$$f_{ud} = f_0 (T/T_{\text{MCT}} - 1)^{3/2}, \quad \text{if } T > T_{\text{MCT}}. \quad (9)$$

The exponent 3/2 in Eq. (9) is the same that describes the approach to the dynamical transition in the mean-field  $p$ -spin model [36]. As in mean-field, a geometric transition occurs indeed at  $T_{\text{MCT}}$ , but it captures the disappearance of delocalized unstable modes only. In finite dimensions, localized modes exist at any temperature and therefore the MCT crossover coincides with a localization transition of unstable modes. We emphasize that the values of  $T_{\text{MCT}}$  were independently determined from power law fits to the relaxation time data elsewhere, see Table 1. The statistical uncertainty on  $f_{ud}$  becomes large, in relative terms, only when approaching the transition from the right.

Figure 1(c) shows that the concentration of localized unstable modes  $f_{ul} = (f_u - f_{ud})$  is system-dependent. We suggest that a higher fraction of localized modes at  $T_{\text{MCT}}$  corresponds to stronger deviations from the geometric transition scenario observed in the mean-field  $p$ -spin model. Liquids that narrowly avoid the geometric transition should display a marked change in dynamic behavior across the MCT crossover temperature. On the other hand, we note that there exist models of glassy dynamics whose PES is, unlike the one of  $p$ -spins, trivial or not smooth and yet display MCT-like dynamics [37–39]. Whether another mechanism can explain the MCT phenomenology in all these systems remains a challenging open question. We expect hard spheres to be similarly characterized by a localization transition of unstable modes in a free-energy landscape, but there exist at present no computational tool to attack this problem. Finally, the trend in Fig. 1(c) superficially suggests a correlation between glass-forming ability [27] and the concentration of localized unstable modes. While intriguing, this observation needs to be tested over a more diverse pool of liquids and also changing the dimensionality of space.

In mean-field  $p$ -spin models, the geometric transition is defined through the relationship between  $f_u$  and the energy  $e_s$  of stationary points. At the transition, stationary points of average energy  $e_{th}$  have a vanishing fraction of unstable modes  $f_u$ :  $f_u(e_{th}) = 0$  [11]. Such a representation reveals an intrinsic property of the landscape and does not depend on the way in which the latter is sampled. In finite-dimensional systems, the  $e_s(f_u)$  relation deviates from the linear behavior observed well above  $T_{\text{MCT}}$  [22, 23] and we confirm these results over a broader temperature range, see Fig. 1(d). These deviations were previously attributed to finite size effects [40], but they actually stem from localized modes. In fact, looking at the relation  $e_s(f_{ud})$  in Fig. 1(e), where the temperature is used as an implicit variable, one observes a geometric transition at a finite energy threshold. The values of the threshold energies  $e_{th}$ , determined as the largest average energy of stationary points such that  $f_{ud}(e_{th}) = 0$ , are reported in Table 1. This behavior is confirmed in all of the models (except the network liquid, see below), and is a direct consequence of the localization transition.

One notable deviation from the pattern described above occurs for a model of a strong tetrahedral network liquid [34], which mimics the structure and dynamics of silica. Even

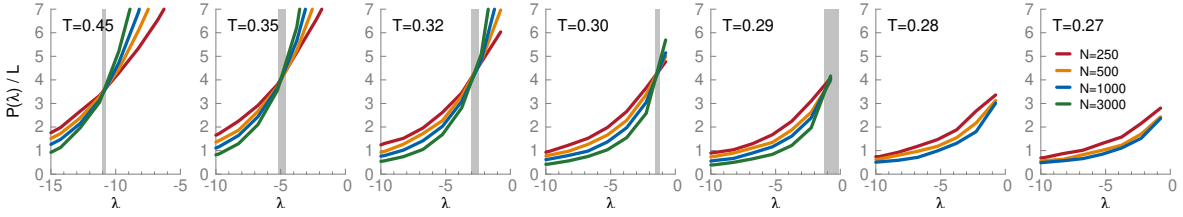


Figure 2: Scaled participation ratio  $P(\lambda, N)/L$  for all studied temperatures and system sizes  $N$  for the ternary mixture model. The mobility edge  $\lambda_e$  is the eigenvalue at which  $P(\lambda, N)/L$  has a fixed point and is indicated by a vertical bar. The width of the vertical bar corresponds to the uncertainty on  $\lambda_e$ .

though the vast majority of unstable modes of this model is localized at any temperature [34], a small fraction of delocalized modes survives even below the putative MCT crossover and no geometric transition is observed in the temperature range accessible to our simulations. While this discrepancy is in line with the conventional Angell picture, which asserts that fragile and strong liquids form two distinct classes [1], it may also be due to the limited temperature range probed by our simulations. Nonetheless, we argue that even if an underlying geometric transition were present in this model, its features would be washed out by the large concentration of localized modes, which corresponds to the elementary rearrangements of the tetrahedral structural units [34]. At a more fundamental level, our results cast some doubts on the relevance of the MCT description of the early stages of glassy dynamics in strong liquids [41, 42], see also [43].

The results presented above rely on our ability to determine the mobility edge of the spectrum, *i.e.* the eigenvalue  $\lambda_e$  that separates localized and delocalized unstable modes. Early attempts to determine the mobility edge from the spectrum of the instantaneous normal modes (INM) in liquids were unsuccessful [44], but the technical problems were recently tackled [45] by applying a finite-size scaling procedure borrowed from the study of Anderson localization [46]. We used this procedure to classify the unstable modes of all studied models. In the following, we illustrate this approach for one specific ternary mixture [32] and provide full details about the remaining systems in the accompanying data set [35].

As a measure of the localization of a mode  $\alpha$ , we consider the participation ratio

$$P_\alpha = \left( \sum_{i=1}^N |\vec{e}_{\alpha,i}|^4 \right)^{-1},$$

where  $\vec{e}_{\alpha,i}$  is the corresponding normalized eigenvector. We then compute the average participation ratio  $P(\lambda, N)$  of modes with eigenvalue  $\lambda$  for a given system size  $N$ . A finite-size scaling analysis allows one to determine the mobility edge  $\lambda_e$  as the fixed point in  $P(\lambda, N)/L$ , where  $L$  is the linear size of the system [45]. The rationale is that, for delocalized modes,  $P$  scales at least linearly with  $L$ , whereas it is independent of  $L$  for localized modes. As a result, the mobility edge identifies the eigenvalue where finite size effects change nature. Localized modes have  $\lambda < \lambda_e$ , while  $\lambda_e < \lambda < 0$  for delocalized modes.

Figure 2 shows  $P(\lambda, N)/L$  across the MCT crossover temperature for the ternary mixture. A well-defined fixed point at  $\lambda_e(T)$  is visible in the participation ratio when  $T > T_{\text{MCT}}$ . The data show that  $\lambda_e$  reaches zero at  $T \approx 0.28$ , which matches well the mode-coupling temperature determined from the dynamics [27]. Below this temperature, the absence of a

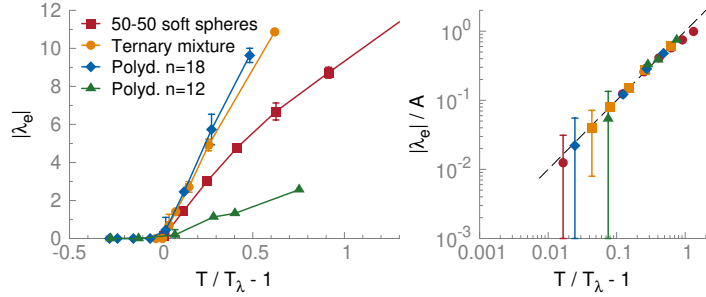


Figure 3: Mobility edge  $|\lambda_e|$  as a function of rescaled temperature for all studied fragile liquids. The localization transition temperature  $T_\lambda$  is extracted from a fit to Eq. (10). Panel (b) shows a log-log representation of  $|\lambda_e|/A$  versus the rescaled temperature. The dashed line represents the identity function.

non-trivial fixed point means that all unstable modes are localized and we formally set  $\lambda_e = 0$ . Quantitatively, the mobility edge of the unstable modes was determined by determining the intersection of pairs of scaled participation ratios  $P(\lambda, L_i)/L_i$  and  $P(\lambda, L_j)/L_j$ , where the indices  $L_i$  and  $L_j$  denote different linear system sizes. The mobility edge  $\lambda_e$  is then defined as the average of the eigenvalues  $\lambda_e^{ij}$  at which the scaled participation ratios cross. If two curves  $P(\lambda, L_i)/L_i$  and  $P(\lambda, L_j)/L_j$  do not intersect each other, the corresponding estimate  $\lambda_e^{ij}$  of the mobility edge is set to zero. The uncertainty on  $\lambda_e$  was estimated as half of the difference between the extreme values of  $\lambda_e^{ij}$ . To determine the uncertainty on the fractions of delocalized and localized unstable modes, we considered the  $\lambda_e$ -dependence of  $f_{ud}(T; \lambda_e)$  and  $f_{ul}(T; \lambda_e)$  respectively, and propagated the uncertainty on  $\lambda_e$ .

In Fig. 3 we show that the mobility edge goes to zero linearly as  $T \rightarrow T_\lambda^+$  for all fragile liquids studied in this work and is zero for  $T < T_\lambda$ . The precise value of the localization temperature  $T_\lambda$  can be extracted from least square fitting of the mobility edge to the following functional form

$$\lambda_e(T) = \begin{cases} A_\lambda(T/T_\lambda - 1) & \text{if } T > T_\lambda \\ 0 & \text{if } T \leq T_\lambda \end{cases} \quad (10)$$

where  $A_\lambda$  and  $T_\lambda$  are adjustable parameters. The values of  $T_\lambda$  are reported in Table 1, they correlate strongly with those of  $T_{\text{MCT}}$ . The localization transition temperature  $T_\lambda$ , at which the mobility edge vanishes, defines a new characteristic temperature for glassy dynamics. It can be determined using a well-defined procedure and subsumes the conventional definition of the mode-coupling crossover based on fitting the dynamic data. Its quantitative determination is only limited by the statistical uncertainty on the mobility edge very close to the transition.

The fraction of delocalized and localized modes shown in Fig. 1 are then defined as  $f_{ud} = \int_{\lambda_e}^{0^-} g(\lambda) d\lambda$  and  $f_{ul} = \int_{-\infty}^{\lambda_e} g(\lambda) d\lambda$ , respectively, where  $g(\lambda)$  is the normalized spectrum of the stationary points <sup>1</sup>. We used the largest system size available for each system to compute the fractions of unstable modes, see [35] for an analysis of finite size effects. Results obtained using INM showed instead that the vast majority of the unstable directions are delocalized at any temperature [45], with no obvious change as  $T \rightarrow T_{\text{MCT}}$ . The INM thus seem unable to capture changes in the landscape properties relevant to the MCT crossover, unless perhaps

<sup>1</sup>The three null modes as well as the as spurious inflection mode of quasi-stationary points [17, 18] are removed from the analysis.

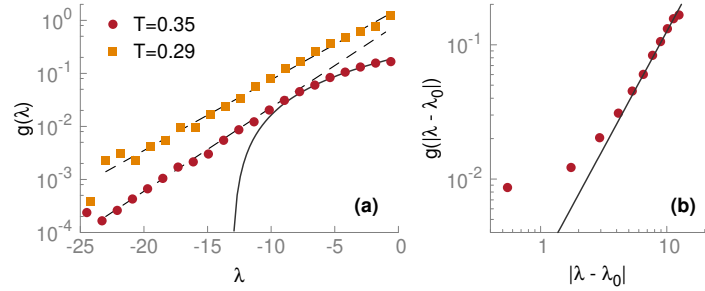


Figure 4: Unstable part of the spectrum  $g(\lambda)$  of stationary points for the ternary mixture. (a)  $g(\lambda)$  at  $T = 0.35$  and  $T = 0.29$ . The data for  $T = 0.29$  are scaled by a factor 5. (b) Log-log representation of  $g(|\lambda - \lambda_0|)$  versus  $|\lambda - \lambda_0|$   $T = 0.35$ . In both panels, the solid line represents the power law  $g(|\lambda - \lambda_0|) = B(|\lambda - \lambda_0|)^{\nu}$ , with  $\lambda_0 = -13.1$ ,  $B = 0.0023$ ,  $\nu = 1.7$ .

by carefully filtering the unstable directions [47].

To corroborate our localization analysis, we consider two additional aspects: the shape of the unstable portion of the spectrum  $g(\lambda)$  and its level spacing statistics. Following Ref. [48], we expect the unstable portion of the spectrum to behave differently depending on localization properties. For  $\lambda_e < \lambda < 0$  and  $T > T_{\text{MCT}}$ , the spectrum should display a power-law behavior  $g(\lambda) \sim (\lambda - \lambda_0)^\nu$ , where  $\lambda_0$  is the lower band edge [48] and  $\lambda \geq \lambda_0$ . This functional form is found in the mean-field  $p$ -spin model and, according to the single-saddle model of Ref. [48], is compatible with the short-time dynamics predicted by MCT. For  $\lambda < \lambda_e$ , we expect instead an exponential tail corresponding to an uncorrelated distribution of localized modes. In Fig. 4 we confirm qualitatively the presence of these two regimes in the spectrum of the stationary and quasi-stationary points sampled at  $T = 0.35 > T_{\text{MCT}}$ . We notice that the crossover between them occurs close to, though somewhat below, the mobility edge  $\lambda_e(T=0.35) \approx -4.9$  determined from the finite size scaling analysis. On the other hand, for  $T < T_{\text{MCT}}$ , the distribution is close to an exponential, as expected for a fully localized spectrum. At first sight, the shape of the unstable spectrum of stationary points appears quite distinct from the one found for soft stable modes [49], which displays a  $g(\omega) \sim \omega^4$  scaling, where  $\omega = \sqrt{|\lambda|}$  is the eigenfrequency. This in turn corresponds to  $g(\lambda) \sim \lambda^{3/2} \approx \lambda^\nu$ , which suggests a possible connection with the shape of the delocalized portion of the unstable spectrum <sup>2</sup>. It would thus be interesting to analyze more carefully the relationship between the unstable modes and the soft stable modes.

A well-established method to distinguish localized and delocalized modes builds on the analysis of the level spacing statistics [50], as used extensively in the analysis of spectra in a variety of problems, including the INM of supercooled and confined liquids [45, 51, 52]. Here we compute the level spacing distribution of stationary and quasi-stationary points of the PES. We first determine the smooth part of the cumulative density of states  $\xi(\lambda)$  through a cubic spline of the raw data and then compute the level spacings  $\tilde{s} = \xi(\lambda_{i+1}) - \xi(\lambda_i)$  from the ordered set of the eigenvalues. Finally, the level spacings are normalized,  $s = \tilde{s}/\langle \tilde{s} \rangle$ . In Fig. 5 we show representative results for the level spacing distribution at  $T = 0.35$ , i.e. in a regime where both kinds of modes can be clearly identified. We find that the level spacing distribution

<sup>2</sup>We thanks M. Shimada for this remark

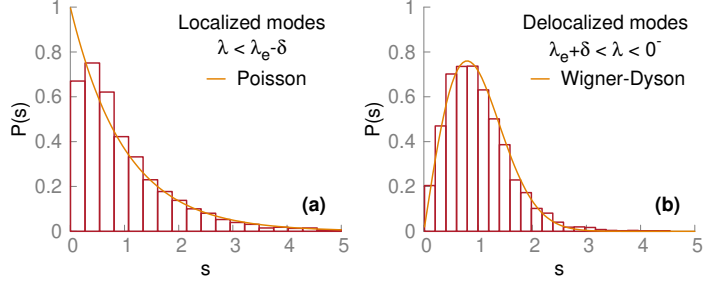


Figure 5: Level spacing statistics at  $T = 0.35$  for (a) localized and (b) delocalized modes in the ternary mixture model. The distribution  $P(s)$  of level spacings  $s$  is computed in the indicated portion of eigenvalues, with  $\delta = 1$ . The full line indicates a Poisson distribution in (a) and a Wigner-Dyson distribution in (b), see text for definitions.

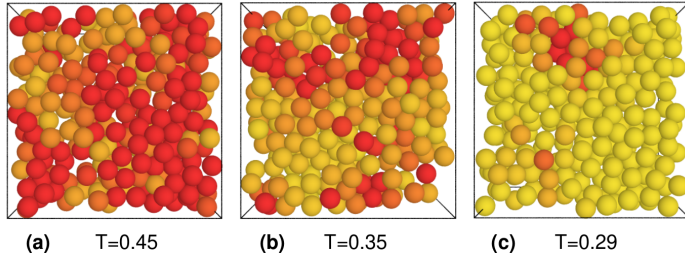


Figure 6: Spatial distribution of the average displacements  $e_i^2$  on the unstable modes for three stationary points sampled in the ternary mixture (a) well above ( $T = 0.45$ ), (b) around ( $T = 0.35$ ) and (c) at the mode-coupling temperature ( $T = 0.29$ ). Only particles in a vertical slab of thickness  $2\sigma$  are shown. The color coding interpolates between yellow (●) for particles with  $e_i^2 = 0$  and red (●) for those with  $e_i^2 \geq 0.04$ .

of the delocalized modes  $\lambda > \lambda_e$  is well described by the Wigner-Dyson distribution

$$P(s) = \left(\frac{\pi s}{2}\right) \exp\left(-\frac{\pi}{4}s^2\right).$$

For the localized modes, the distribution is close to the Poisson distribution expected for uncorrelated eigenvalues,  $P(s) = \exp(-s)$ , although there remains a small depletion at small level spacings. The trend of the distributions for varying  $N$  (not shown) suggests that this depletion may be a finite size effect. Overall, the analysis of the level spacing statistics confirms the localization transition of the unstable modes.

Finally, we make a direct contact with the real space structure of the modes and inspect the average displacements on the unstable modes  $e_i^2 = (1/n_u) \sum_{\alpha} |\vec{e}_{\alpha,i}|^2$ . Since each eigenvector is normalized, we have  $e_i^2 < 1$ . By averaging over all unstable modes, the instability field  $e_i^2$  captures the degree of localization of a given stationary point. The three snapshots in Fig. 6 depict the spatial distribution of  $e_i^2$  for representative saddle points. On approaching  $T_{\text{MCT}}$ , the instability field becomes localized around few isolated particles with large displacements. Early simulations [53] found a correlation between  $e_i^2$  and the short-time dynamical heterogeneity of a Lennard-Jones mixture. Our results suggest that the growth of dynamic correlations associated to the progressive stabilization of unstable modes as  $T \rightarrow T_{\text{MCT}}$  is cut off

because unstable modes become localized, which suggests a plausible explanation for the non-monotonic evolution of dynamic correlations across  $T_{\text{MCT}}$  observed in some liquids [28,54–56]. Since localized modes are present at any temperature, see Fig. 1(c), supercooled liquids may display activated dynamics between nearest energy minima even above  $T_{\text{MCT}}$ , at variance with the traditional Goldstein’s scenario [8] but in agreement with studies on the metabasin structure of the landscape [21] and on dynamic facilitation [19].

## 5 Conclusions

In conclusion, we found that the localization properties of unstable directions of the potential energy landscape of several models of glasses display a marked change close to the mode-coupling crossover temperature  $T_{\text{MCT}}$ . Our observations demonstrate that the geometric transition found in mean-field models and investigated in early simulation studies [9–11] involves only the subset of delocalized unstable modes. The mode-coupling crossover thus corresponds to a localization transition and is a meaningful physical concept only if the concentration of localized unstable modes is sufficiently low. These results may provide guidelines to understand the dynamic crossovers reported in some supercooled liquids by experiments [57,58] and simulations [28,54–56]. In liquids characterized by a high concentration of localized unstable modes, including *e.g.* strong glass-formers, the physics should be controlled instead by localized excitations, even above  $T_{\text{MCT}}$ . Kinetically constrained models [59] could then provide an effective theoretical framework to account for the build up of dynamic correlations from such localized rearrangements. Liquids embedded in higher dimensions, which have recently received significant interest, are closer to mean-field behavior and we predict that they will display small concentrations of localized modes and be structurally very homogeneous. These expectations are consistent with recent findings for a nearly mean-field three-dimensional model [60], and can now be tested numerically in large dimensions [61]. Future studies should also focus on generalizing the analysis to models of experimentally relevant models of molecular liquids.

## Acknowledgements

We thank A. Ikeda, W. Kob, M. Ozawa, G. Pastore, M. Shimada and G. Tarjus for useful discussions. Data and workflow relevant to this work will be available after publication at <https://doi.org/10.5281/zenodo.1478601>. This work was supported by a grant from the Simons Foundation (# 454933, L. Berthier).

## A Quasi-stationary points versus stationary points

In this section we compare the statistical properties of quasi-stationary and stationary points for the ternary mixture. We focus on this model because it is the one for which we accumulated the largest statistics.

The geometric plot  $e_s(f_u)$  in Fig. 7 shows results obtained separately for stationary points and for the bulk of the points obtained from  $W$ -minimizations. Only minor discrepancies

between the two sets of data are visible, the fraction of unstable modes being slightly smaller in stationary points at small  $e_s$ .

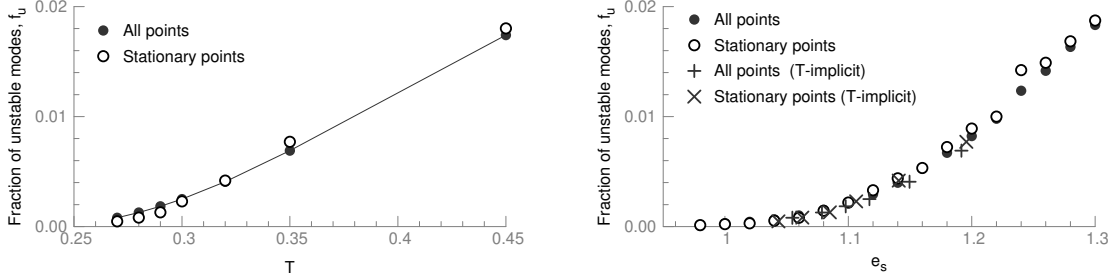


Figure 7: Fraction of unstable modes in all points and in true stationary points obtained from  $W$ -minimizations as function of (a) temperature and (b) energy. In panel (b) we show both averages on a per-energy basis and using  $T$  as an implicit variable. The number of particles is  $N = 500$ .

In Fig. 8 we show the participation ratio  $P(\lambda)$  of the unstable modes for all points obtained from all  $W$ -minimizations and for stationary points only. The two sets of data are consistent with one another, with only minor discrepancies below the mode-coupling temperature  $T_{MCT} = 0.29$ . A plot of the average participation ratio as a function of the fraction  $f_u$  shows a good data collapse of the two sets of data (not shown).

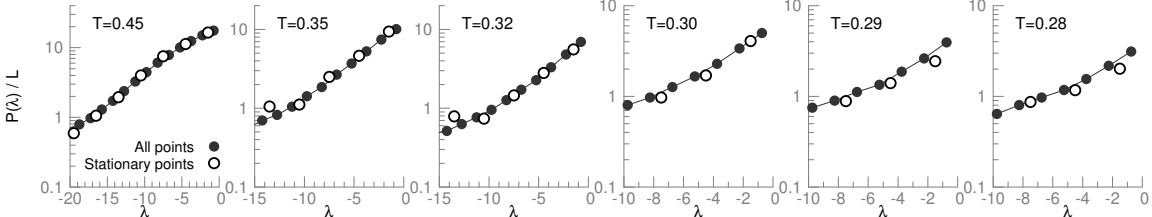


Figure 8: Scaled participation ratio  $P(\lambda)/L$  as a function of  $\lambda$  for the ternary mixture for all points obtained from  $W$ -minimizations (filled circles) and for stationary points only (empty circles). The number of particles is  $N = 500$ .

In Fig. 9 we show the fraction of delocalized unstable modes for stationary points only, *i.e.* without quasi-stationary points. We use the mobility edge obtained from analysis of all  $W$ -minimizations because the current statistics on the participation ratio is not sufficient to determine the mobility edge. The data are fairly consistent with the approximate master curve determined from both stationary and quasi-stationary points. Overall the trend confirms the localization transition of the stationary points at the mode-coupling temperature.

## References

[1] C. A. Angell, *Formation of Glasses from Liquids and Biopolymers*, Science **267**, 1924 (1995), doi:[10.1126/science.267.5206.1924](https://doi.org/10.1126/science.267.5206.1924).

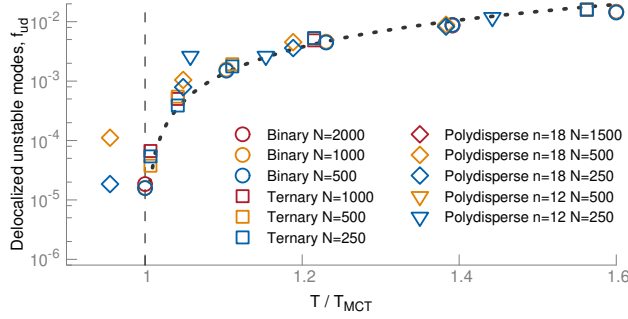


Figure 9: Fraction of delocalized unstable modes  $f_{ud}$  as a function of  $T/T_{MCT}$  for stationary points only, in all studied models except the network-forming liquid. The system size  $N$  is indicated in the legend. The dotted line indicates the approximate master curve, Eq.1 in the main text, obtained from all points.

- [2] L. Berthier and M. D. Ediger, *Facets of glass physics*, Phys. Today **69**, 40 (2016), doi:[10.1063/PT.3.3052](https://doi.org/10.1063/PT.3.3052).
- [3] A. Cavagna, *Supercooled liquids for pedestrians*, Phys. Rep. **476**, 51 (2009), doi:[10.1016/j.physrep.2009.03.003](https://doi.org/10.1016/j.physrep.2009.03.003).
- [4] L. Berthier and G. Biroli, *Theoretical perspective on the glass transition and amorphous materials*, Rev. Mod. Phys. **83**, 587 (2011), doi:[10.1103/RevModPhys.83.587](https://doi.org/10.1103/RevModPhys.83.587).
- [5] C. P. Royall, F. Turci, S. Tatsumi, J. Russo and J. Robinson, *The race to the bottom: Approaching the ideal glass?*, J. Phys.: Condens. Matter **30**, 363001 (2018), doi:[10.1088/1361-648X/aad10a](https://doi.org/10.1088/1361-648X/aad10a).
- [6] W. Götze, *Complex Dynamics of Glass-Forming Liquids: A Mode-Coupling Theory*, Oxford University Press, USA (2009).
- [7] T. R. Kirkpatrick and D. Thirumalai, *Comparison between dynamical theories and metastable states in regular and glassy mean-field spin models with underlying first-order-like phase transitions*, Phys. Rev. A **37**, 4439 (1988), doi:[10.1103/PhysRevA.37.4439](https://doi.org/10.1103/PhysRevA.37.4439).
- [8] A. Cavagna, *Fragile vs . strong liquids: A saddles-ruled scenario*, EPL (Europhysics Letters) **53**(4), 490 (2001).
- [9] K. Broderix, K. K. Bhattacharya, A. Cavagna, A. Zippelius and I. Giardina, *Energy Landscape of a Lennard-Jones Liquid: Statistics of Stationary Points*, Phys. Rev. Lett. **85**, 5360 (2000), doi:[10.1103/PhysRevLett.85.5360](https://doi.org/10.1103/PhysRevLett.85.5360).
- [10] L. Angelani, R. Di Leonardo, G. Ruocco, A. Scala and F. Sciortino, *Saddles in the Energy Landscape Probed by Supercooled Liquids*, Phys. Rev. Lett. **85**, 5356 (2000), doi:[10.1103/PhysRevLett.85.5356](https://doi.org/10.1103/PhysRevLett.85.5356).
- [11] T. S. Grigera, A. Cavagna, I. Giardina and G. Parisi, *Geometric Approach to the Dynamic Glass Transition*, Phys. Rev. Lett. **88**, 055502 (2002), doi:[10.1103/PhysRevLett.88.055502](https://doi.org/10.1103/PhysRevLett.88.055502).

- [12] L. Angelani, R. Di Leonardo, G. Ruocco, A. Scala and F. Sciortino, *Quasisaddles as relevant points of the potential energy surface in the dynamics of supercooled liquids*, *J. Chem. Phys.* **116**, 10297 (2002), doi:[10.1063/1.1475764](https://doi.org/10.1063/1.1475764).
- [13] G. Fabricius and D. A. Stariolo, *Distance between inherent structures and the influence of saddles on approaching the mode coupling transition in a simple glass former*, *Phys. Rev. E* **66**, 031501 (2002), doi:[10.1103/PhysRevE.66.031501](https://doi.org/10.1103/PhysRevE.66.031501).
- [14] J. Kurchan and L. Laloux, *Phase space geometry and slow dynamics*, *J. Phys. A: Math. Gen.* **29**, 1929 (1996), doi:[10.1088/0305-4470/29/9/009](https://doi.org/10.1088/0305-4470/29/9/009).
- [15] A. Cavagna, I. Giardina and G. Parisi, *Stationary points of the Thouless-Anderson-Palmer free energy*, *Phys. Rev. B* **57**, 11251 (1998), doi:[10.1103/PhysRevB.57.11251](https://doi.org/10.1103/PhysRevB.57.11251).
- [16] L. Angelani, G. Ruocco, M. Sampoli and F. Sciortino, *General features of the energy landscape in Lennard-Jones-like model liquids*, *J. Chem. Phys.* **119**, 2120 (2003), doi:[10.1063/1.1587132](https://doi.org/10.1063/1.1587132).
- [17] J. P. K. Doye and D. J. Wales, *Saddle points and dynamics of Lennard-Jones clusters, solids, and supercooled liquids*, *J. Chem. Phys.* **116**, 3777 (2002), doi:[10.1063/1.1436470](https://doi.org/10.1063/1.1436470).
- [18] J. P. K. Doye and D. J. Wales, *Comment on “Quasisaddles as relevant points of the potential energy surface in the dynamics of supercooled liquids” [J. Chem. Phys. 116, 10297 (2002)]*, *J. Chem. Phys.* **118**, 5263 (2003), doi:[10.1063/1.1553754](https://doi.org/10.1063/1.1553754).
- [19] L. Berthier and J. P. Garrahan, *Real space origin of temperature crossovers in supercooled liquids*, *Phys. Rev. E* **68**, 041201 (2003), doi:[10.1103/PhysRevE.68.041201](https://doi.org/10.1103/PhysRevE.68.041201).
- [20] D. J. Wales and J. P. K. Doye, *Stationary points and dynamics in high-dimensional systems*, *J. Chem. Phys.* **119**, 12409 (2003), doi:[10.1063/1.1625644](https://doi.org/10.1063/1.1625644).
- [21] B. Doliwa and A. Heuer, *Energy barriers and activated dynamics in a supercooled Lennard-Jones liquid*, *Phys. Rev. E* **67**, 031506 (2003), doi:[10.1103/PhysRevE.67.031506](https://doi.org/10.1103/PhysRevE.67.031506).
- [22] D. Coslovich and G. Pastore, *Understanding fragility in supercooled Lennard-Jones mixtures. II. Potential energy surface*, *J. Chem. Phys.* **127**, 124505 (2007), doi:[10.1063/1.2773720](https://doi.org/10.1063/1.2773720).
- [23] M. Ozawa, W. Kob, A. Ikeda and K. Miyazaki, *Equilibrium phase diagram of a randomly pinned glass-former*, *Proc. Natl. Acad. Sci.* **112**, 6914 (2015), doi:[10.1073/pnas.1500730112](https://doi.org/10.1073/pnas.1500730112).
- [24] D. Gazzillo and G. Pastore, *Equation of state for symmetric non-additive hard-sphere fluids: An approximate analytic expression and new Monte Carlo results*, *Chem. Phys. Lett.* **159**, 388 (1989), doi:[10.1016/0009-2614\(89\)87505-0](https://doi.org/10.1016/0009-2614(89)87505-0).
- [25] T. S. Grigera and G. Parisi, *Fast Monte Carlo algorithm for supercooled soft spheres*, *Phys. Rev. E* **63**, 045102 (2001), doi:[10.1103/PhysRevE.63.045102](https://doi.org/10.1103/PhysRevE.63.045102).
- [26] L. Berthier, D. Coslovich, A. Ninarello and M. Ozawa, *Equilibrium Sampling of Hard Spheres up to the Jamming Density and Beyond*, *Phys. Rev. Lett.* **116**, 238002 (2016), doi:[10.1103/PhysRevLett.116.238002](https://doi.org/10.1103/PhysRevLett.116.238002).

[27] A. Ninarello, L. Berthier and D. Coslovich, *Models and Algorithms for the Next Generation of Glass Transition Studies*, Phys. Rev. X **7**, 021039 (2017), doi:[10.1103/PhysRevX.7.021039](https://doi.org/10.1103/PhysRevX.7.021039).

[28] L. Berthier, G. Biroli, D. Coslovich, W. Kob and C. Toninelli, *Finite-size effects in the dynamics of glass-forming liquids*, Phys. Rev. E **86**, 031502 (2012), doi:[10.1103/PhysRevE.86.031502](https://doi.org/10.1103/PhysRevE.86.031502).

[29] D. C. Liu and J. Nocedal, Math. Program. **45**, 503 (1989).

[30] M. Sampoli, P. Benassi, R. Eramo, L. Angelani and G. Ruocco, *The potential energy landscape in the Lennard-Jones binary mixture model*, J. Phys. Condens. Matter **15**, S1227 (2003), doi:[10.1088/0953-8984/15/11/340](https://doi.org/10.1088/0953-8984/15/11/340).

[31] B. Bernu, J. P. Hansen, Y. Hiwatari and G. Pastore, *Soft-sphere model for the glass transition in binary alloys: Pair structure and self-diffusion*, Phys. Rev. A **36**, 4891 (1987), doi:[10.1103/PhysRevA.36.4891](https://doi.org/10.1103/PhysRevA.36.4891).

[32] R. Gutiérrez, S. Karmakar, Y. G. Pollack and I. Procaccia, *The static lengthscale characterizing the glass transition at lower temperatures*, EPL **111**, 56009 (2015), doi:[10.1209/0295-5075/111/56009](https://doi.org/10.1209/0295-5075/111/56009).

[33] S. Karmakar, E. Lerner, I. Procaccia and J. Zylberg, *Effect of the interparticle potential on the yield stress of amorphous solids*, Phys. Rev. E **83**, 046106 (2011), doi:[10.1103/PhysRevE.83.046106](https://doi.org/10.1103/PhysRevE.83.046106).

[34] D. Coslovich and G. Pastore, *Dynamics and energy landscape in a tetrahedral network glass-former: Direct comparison with models of fragile liquids*, J. Phys. Condens. Matter **21**, 285107 (2009), doi:[10.1088/0953-8984/21/28/285107](https://doi.org/10.1088/0953-8984/21/28/285107).

[35] *Data set and workflow for “A localization transition underlies the mode-coupling crossover of glasses”*, doi:[10.5281/zenodo.1478601](https://doi.org/10.5281/zenodo.1478601).

[36] A. Cavagna, I. Giardina and G. Parisi, *Role of saddles in mean-field dynamics above the glass transition*, J. Phys. A: Math. Gen. **34**, 5317 (2001), doi:[10.1088/0305-4470/34/26/302](https://doi.org/10.1088/0305-4470/34/26/302).

[37] C. Renner, H. Löwen and J.-L. Barrat, *Orientational glass transition in a rotator model*, Phys. Rev. E **52**, 5091 (1995), doi:[10.1103/PhysRevE.52.5091](https://doi.org/10.1103/PhysRevE.52.5091).

[38] K. Kawasaki and B. Kim, *Exactly solvable toy model that mimics the mode coupling theory of supercooled liquid and glass transition*, Phys. Rev. Lett. **86**, 3582 (2001), doi:[10.1103/PhysRevLett.86.3582](https://doi.org/10.1103/PhysRevLett.86.3582).

[39] M. Sellitto, *Crossover from  $\beta$  to  $\alpha$  relaxation in cooperative facilitation dynamics*, Phys. Rev. Lett. **115**, 225701 (2015), doi:[10.1103/PhysRevLett.115.225701](https://doi.org/10.1103/PhysRevLett.115.225701).

[40] T. S. Grigera, *Geometrical properties of the potential energy of the soft-sphere binary mixture*, J. Chem. Phys. **124**, 064502 (2006), doi:[10.1063/1.2151899](https://doi.org/10.1063/1.2151899).

[41] J. Horbach and W. Kob, *Static and dynamic properties of a viscous silica melt*, Phys. Rev. B **60**, 3169 (1999), doi:[10.1103/PhysRevB.60.3169](https://doi.org/10.1103/PhysRevB.60.3169).

[42] F. Sciortino and W. Kob, *Debye-waller factor of liquid silica: Theory and simulation*, Phys. Rev. Lett. **86**, 648 (2001).

[43] L. Berthier, *Revisiting the slow dynamics of a silica melt using Monte Carlo simulations*, Phys. Rev. E **76**, 011507 (2007), doi:[10.1103/PhysRevE.76.011507](https://doi.org/10.1103/PhysRevE.76.011507).

[44] S. D. Bembenek and B. B. Laird, *The role of localization in glasses and supercooled liquids*, J. Chem. Phys. **104**, 5199 (1996), doi:[10.1063/1.471147](https://doi.org/10.1063/1.471147).

[45] V. I. Clapa, T. Kottos and F. W. Starr, *Localization transition of instantaneous normal modes and liquid diffusion*, J. Chem. Phys. **136**, 144504 (2012), doi:[doi:10.1063/1.3701564](https://doi.org/10.1063/1.3701564).

[46] B. I. Shklovskii, B. Shapiro, B. R. Sears, P. Lambrianides and H. B. Shore, *Statistics of spectra of disordered systems near the metal-insulator transition*, Phys. Rev. B **47**, 11487 (1993), doi:[10.1103/PhysRevB.47.11487](https://doi.org/10.1103/PhysRevB.47.11487).

[47] C. Donati, F. Sciortino and P. Tartaglia, *Role of Unstable Directions in the Equilibrium and Aging Dynamics of Supercooled Liquids*, Phys. Rev. Lett. **85**, 1464 (2000), doi:[10.1103/PhysRevLett.85.1464](https://doi.org/10.1103/PhysRevLett.85.1464).

[48] A. Cavagna, I. Giardina and T. S. Grigera, *A single saddle model for the -relaxation in supercooled liquids*, J. Phys. A: Math. Gen. **36**, 10721 (2003), doi:[10.1088/0305-4470/36/43/004](https://doi.org/10.1088/0305-4470/36/43/004).

[49] E. Lerner, G. Düring and E. Bouchbinder, *Statistics and Properties of Low-Frequency Vibrational Modes in Structural Glasses*, Phys. Rev. Lett. **117**, 035501 (2016), doi:[10.1103/PhysRevLett.117.035501](https://doi.org/10.1103/PhysRevLett.117.035501).

[50] T. Guhr, A. Müller-Groeling and H. A. Weidenmüller, *Random-matrix theories in quantum physics: Common concepts*, Phys. Rep. **299**, 189 (1998), doi:[10.1016/S0370-1573\(97\)00088](https://doi.org/10.1016/S0370-1573(97)00088).

[51] S. Ciliberti and T. S. Grigera, *Localization threshold of instantaneous normal modes from level-spacing statistics*, Phys. Rev. E **70**, 061502 (2004), doi:[10.1103/PhysRevE.70.061502](https://doi.org/10.1103/PhysRevE.70.061502).

[52] B. Ash, C. Dasgupta and A. Ghosal, *Analysis of vibrational normal modes for Coulomb clusters*, Phys. Rev. E **98**, 042134 (2018), doi:[10.1103/PhysRevE.98.042134](https://doi.org/10.1103/PhysRevE.98.042134).

[53] D. Coslovich and G. Pastore, *Are there localized saddles behind the heterogeneous dynamics of supercooled liquids?*, Europhys. Lett **75**, 784 (2006), doi:[10.1209/eppl/10175-8](https://doi.org/10.1209/epl/i2006-10175-8).

[54] W. Kob, S. Roldán-Vargas and L. Berthier, *Non-monotonic temperature evolution of dynamic correlations in glass-forming liquids*, Nat. Phys. **8**, 164 (2012), doi:[10.1038/nphys2133](https://doi.org/10.1038/nphys2133).

[55] E. Flenner and G. Szamel, *Dynamic heterogeneities above and below the mode-coupling temperature: Evidence of a dynamic crossover*, J. Chem. Phys. **138**, 12A523 (2013), doi:[doi:10.1063/1.4773321](https://doi.org/10.1063/1.4773321).

- [56] D. Coslovich, M. Ozawa and W. Kob, *Dynamic and thermodynamic crossover scenarios in the Kob-Andersen mixture: Insights from multi-CPU and multi-GPU simulations*, Eur. Phys. J. E **41**, 62 (2018), doi:[10.1140/epje/i2018-11671](https://doi.org/10.1140/epje/i2018-11671).
- [57] F. Stickel, E. W. Fischer and R. Richert, *Dynamics of glass-forming liquids. I. Temperature-derivative analysis of dielectric relaxation data*, J. Chem. Phys. **102**, 6251 (1995), doi:[10.1063/1.469071](https://doi.org/10.1063/1.469071).
- [58] V. N. Novikov and A. P. Sokolov, *Qualitative change in structural dynamics of some glass-forming systems*, Phys. Rev. E **92**, 062304 (2015), doi:[10.1103/PhysRevE.92.062304](https://doi.org/10.1103/PhysRevE.92.062304).
- [59] A. Keys, L. O. Hedges, J. P. Garrahan, S. C. Glotzer and D. Chandler, *Excitations Are Localized and Relaxation Is Hierarchical in Glass-Forming Liquids*, Phys. Rev. X **1**, 021013 (2011), doi:[10.1103/PhysRevX.1.021013](https://doi.org/10.1103/PhysRevX.1.021013).
- [60] D. Coslovich, A. Ikeda and K. Miyazaki, *Mean-field dynamic criticality and geometric transition in the Gaussian core model*, Phys. Rev. E **93**, 042602 (2016), doi:[10.1103/PhysRevE.93.042602](https://doi.org/10.1103/PhysRevE.93.042602).
- [61] L. Berthier, P. Charbonneau and J. Kundu, *Bypassing sluggishness: Swap algorithm and glassiness in high dimensions*, Phys. Rev. E **99**, 031301 (2019), doi:[10.1103/PhysRevE.99.031301](https://doi.org/10.1103/PhysRevE.99.031301).